Suppressing the efficiency roll-off in thermally-activated-delayed-fluorescence—sensitized fluorescent OLEDs by triplet management under pulsed operation

Rui Chen,[1,2] Yincai Xu,[3] Zeyang Zhou,[1,2] Hong Wang,[1,2] Yueqian Jia,[1,2] Qingda Chang,[1,2]
Pengfei Jin,[1,2] Baipeng Yin,[1] Chenglong Li,[3,*] and Chuang Zhang[1,†]

[1]*Key Laboratory of Photochemistry, Beijing National Laboratory for Molecular Sciences, Institute of Chemistry, Chinese Academy of Sciences, Beijing 100190, China*
[2]*University of Chinese Academy of Sciences, Beijing 100049, China*
[3]*Chongqing Research Institute, Jilin University, Changchun 130012, China*

Thermally-activated-delayed-fluorescence (TADF)—sensitized fluorescent organic light-emitting diodes (TSF OLEDs) can simultaneously exhibit high quantum efficiency and high color purity. However, the long-lived nature of excited states during a reverse intersystem-crossing (RISC) process may result in the accumulation and annihilation of triplets and consequently the efficiency roll-off in TSF OLEDs under high current density. In this study, we demonstrate that the pulsed operation of TSF OLEDs can suppress the efficiency roll-off by manipulating exciton dynamics to reduce the accumulation of triplets. Under pulsed operation, the on-cycle luminance of 5CzBN-based OLEDs is increased from 31 370 to 55 760 cd m^{-2} at an amplitude of 10 V, accompanied by an enhancement on on-cycle external quantum efficiency by approximately 100% at a high current density of 1 A cm^{-2}. Exciton dynamics analysis on transient EL curves reveals that the triplet annihilation becomes predominated over the RISC process after the time delay of 1–2 μs, offering a time window for pulse operation. The competition between triplet annihilation and RISC is further investigated by the magnetoelectroluminescence measurement, which confirms that the pulsed operation suppresses the triplet annihilation and thereby improves the conversion from triplets to singlets through RISC. These results show that the on-cycle electroluminescence performance of various TSF OLEDs can be optimized by tuning the pulsed operation parameters according to exciton dynamics, and provide an alternative way to address the issue of efficiency roll-off in next-generation OLEDs.

I. INTRODUCTION

Over the past two decades, significant progress has been made in harvesting electrically generated triplet excitons, leading to the development of strategies for the fabrication of high-efficiency organic light-emitting diodes (OLEDs) [1]. Fluorescent OLEDs with singlet-only emission suffer from the limitation of 25% quantum efficiency as they cannot recycle nonradiative triplets, although they usually exhibit low-efficiency roll-off [2]. The introduction of a thermally activated delayed fluorescence (TADF) sensitizer, where dark triplets can be converted into emissive singlets via reverse intersystem crossing (RISC), into the host-emitter devices, namely TADF-sensitized fluorescent OLEDs (TSF OLEDs), has been proven to show a nearly 100% quantum efficiency [3–9]. However, the RISC process leads to a prolonged lifetime of excitons up to tens of microseconds, which may lead to the accumulation of long-lived triplets and consequently the efficiency roll-off at high current densities [10–12]. The high injection condition favors the bimolecular processes, such as singlet-triplet annihilation (STA) and triplet-triplet annihilation (TTA), which dominate over the monomolecular RISC process and lead to the loss of excitons [13–17]. Previous studies show that the management of triplet accumulation is crucial to suppress the efficiency roll-off, by either the triplet-to-singlet conversion via rapid RISC [18,19] or the triplet-triplet energy transfer to minimize the interaction of triplet excitons [20,21]. A universal yet facile strategy to realize triplet management during the operation of TSF OLEDs is still missing.

Using short electrical pulses to drive OLEDs and recording transient electroluminescence (EL) responses have been adopted as a powerful tool to study the exciton

*chenglongli@jlu.edu.cn
†zhangc@iccas.ac.cn

dynamics, and it is also highly relevant for the realization of electrically driven organic lasers using OLED pump sources [22–24]. In principle, the generation of singlets under electrical injection reaches maximum within a few nanoseconds and they undergo a rapid radiative decay pathway, while the triplets could exist for microseconds and decay nonradiatively [25]. In TSF OLEDs, triplets can participate in the RISC process and thus contribute to an increase in external quantum efficiency (EQE), meanwhile the accumulation of long-lived excitons enables the triplet annihilation process to quench the EL emission. Due to their distinct nature of monomolecular and bimolecular processes, the rate of RISC is linearly dependent on exciton density, and that of the triplet annihilation process shows a nonlinear quadratic dependence on exciton density [26,27]. As triplet excitons accumulate over microseconds, the rate of triplet annihilation experiences a substantial increase compared to the linearly rising rate of RISC. Hence, it should be feasible to employ the pulsed operation to suppress the efficiency roll-off in TSF OLEDs by controlling the triplets at a certain level, where the RISC process dominates over triplet annihilation.

In this work, we propose a triplet management strategy by using the pulsed operation to suppress efficiency roll-off in TSF OLEDs by reducing the accumulation and annihilation of triplets. Micro TSF OLEDs are fabricated to minimize the *RC* effect and meet the requirement of pulsed operation. By employing the pulsed operation as the driving method, the on-cycle luminance of TSF OLEDs is significantly increased from 31 370 to 55 760 cd m^{-2} at an amplitude of 10 V, accompanied by a substantial rise in on-cycle EQE improved by 100% at a current density of 1 A cm^{-2}. The transient EL response in TSF OLEDs under pulsed operation exhibits an increment followed by a relaxation to steady state, simulated on which the exciton dynamics indicate that triplet annihilation becomes dominant over RISC after 1–2 μs of the pulse. Magneto electroluminescence (MEL) is used to study the competition between RISC and triplet annihilation, where the spin-conversion process and exciton interaction are estimated by the signal and amplitude of MEL, respectively. The time-resolved MEL suggests that the RISC process dominates during the initial few hundred nanoseconds of the pulse, confirming the pulsed operation is beneficial to suppress the triplet annihilation. These findings reveal the impact pulsed operation on triplet exciton behavior, offering a possible approach for achieving OLEDs with low efficiency roll-off.

II. RESULTS AND DISCUSSION

A. The energy-transfer process in TSF OLEDs

As shown in Scheme 1, TSF OLEDs feature an emitting layer comprised of a ternary system that includes a
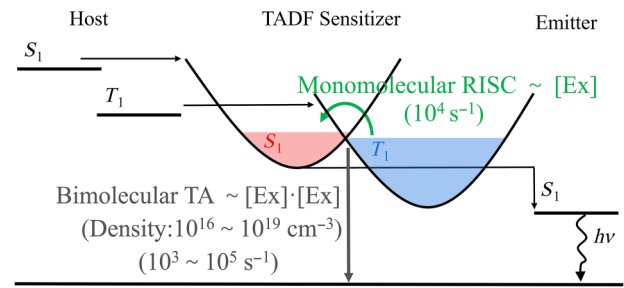
SCHEME 1. The energy levels and energy transfer process in TSF OLEDs.

wide-energy-gap host, a TADF sensitizer, and a narrowband emitter. Electric injection produces 25% singlets and 75% triplets on the host initially, and then transferred to the lowest singlet (S_1) state and the lowest triplet (T_1) state of the TADF sensitizer through energy transfer, respectively. The triplets on the TADF are converted to singlets through RISC and subsequently transferred to the $S1$ of the narrowband emitter, leading to the high efficiency and high color purity in TSF OLEDs. On the other hand, the RISC process prolongs the excited-state lifetime, leading to the triplet accumulation and annihilation. For the monomolecular RISC process (rate constant: 10^3–10^4 s^{-1}), the rate is linearly dependent on the density of triplet excitons, while for the triplet annihilation (TA), the rate of bimolecular process (typical rate constant: 10^{-10} cm^3 s^{-1} for STA and 10^{-15} cm^3 s^{-1} for TTA) exhibits a quadratic dependence on the triplet density, resulting in the rate of triplet annihilation being lower or higher than the RISC rate at lower or higher exciton densities, respectively [28]. On the other hand, the singlet excitons reach their maximum within nanoseconds, while the triplet excitons accumulate over several microseconds. This makes it feasible to suppress the efficiency roll-off in TSF OLEDs by the pulsed operation to control triplet density at a low level, where RISC dominates over triplet annihilation.

B. The performance of micro TSF OLEDs under dc and pulsed operations

Figure 1(a) illustrates the structure of the high-speed OLED, a micro TSF OLED confined by a PMMA template, which consists of a 150-nm-thick ITO anode on a glass substrate followed by a 30-nm-thick NPD as hole transport layer, a 40-nm-thick emissive layer comprised of 90 wt% CBP as the host, 10 wt% 5CzBN as the TADF sensitizer and 1 wt% t-DABNA as the emitter, a 30-nm-thick TPBi as the electron-transport layer capped by a LiF (1.2 nm)/Al (100 nm) cathode (the molecular structures of materials are shown in Fig. S1 within the Supplemental Material [29]). As shown in Fig. S2 within the Supplemental Material [29], the HOMO and LUMO energy levels
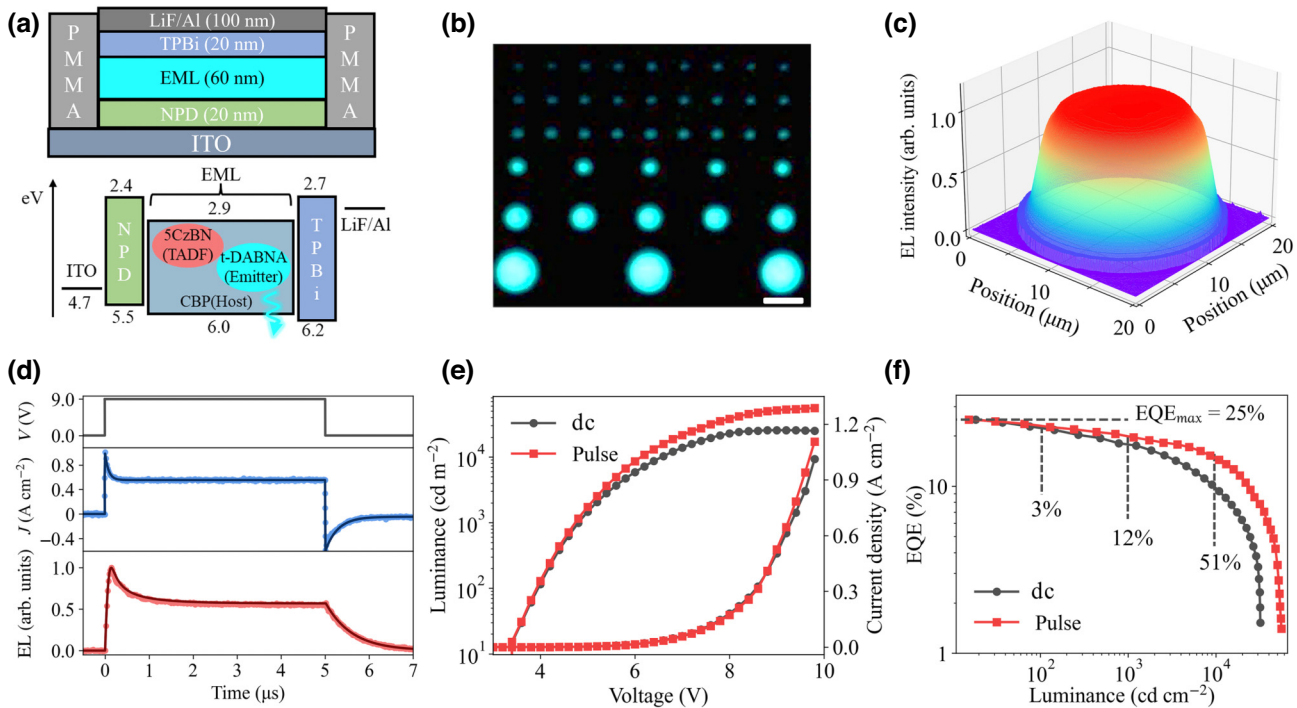
FIG. 1. (a) The device architecture and the energy-level diagram of micro TSF OLEDs. (b) Optical microscopic images of TSF OLEDs with various active areas. Scale bars are 10 μm. (c) The EL intensity profile of the TSF OLED at a current density of 1 A cm^{-2}. (d) The transient current and EL responses of TSF OLEDs under a pulse with an amplitude of 9 V. Pulse excitation: pulse width of 5 μs, repetition frequency of 10 kHz, duty ratio of 5%. The dots and lines represent the experimental data points and fitting curves, respectively. (e) *J-V-L* curves measured from TSF OLEDs under dc and pulsed operation. (f) Plots of EQE versus on-cycle luminance in TSF OLEDs under dc and pulsed operation. Pulse excitation in (e),(f): pulse width of 0.5 μs, repetition frequency of 100 kHz, duty ratio of 5%.

for CBP, 5CzBN, and t-DABNA are 6.0/2.9, 5.6/2.8, and 5.4/2.9 electron volts (eV), respectively. The steady-state PL spectra and PL decay curves of CBP host, TADF sensitizers, t-DABNA and their blended films indicate that the TADF sensitizer is necessary for effective energy transfer to t-DABNA (Figs. S3 and S4 within the Supplemental Material [29]). The device areas of the OLEDs are reduced to severe square micrometers to minimize the *RC* response distortion by reducing the geometrical capacitance [30]. As shown in Fig. 1(b), a series of microsized OLEDs with different area sizes was fabricated [31–33], allowing for the parameter optimization to meet the requirement of the pulsed operation. The *RC* time reaches 68 ns when the active area is reduced to 64 μm^2 and remains for smaller devices (Fig. S5 within the Supplemental Material [29]), which is notably below the lifetime of triplet population evolution. The EL intensity profile in Fig. 1(c) confirms that the micro TSF OLEDs are spatially uniform and do not exhibit hot spots or edge effects.

The performance of TSF OLEDs under pulsed operation is demonstrated by the transient current and EL responses, as shown in Fig. 1(d). When the device is pumped at a pulse with amplitude of 9 V, width of 5 μs, and duty ratio

of 5%, the transient current exhibits an *RC* effect-induced spike upon pulse onset, followed by a rapid relaxation to the steady state within 68 ns. The initial spike indicates the charging process, which fills the equivalent capacitance of TSF OLEDs, while a discharging process is also observed after the pulse [Fig. S6(a) within the Supplemental Material [29]]. The charging or discharging process does not contribute to the carrier recombination for electroluminescence. A peak is also observed in the transient EL response but lasts for more than 1 μs, indicating that the transient EL response originates from the exciton dynamics rather than the *RC* effect. The peak in transient EL curves is attributed to the fact that the singlets rapidly reach the maximum density, but are then quenched by the triplet accumulation and annihilation [34]. This observation suggests that the on-cycle EL performance can be enhanced by operating the device under the pulsed operation. Meanwhile, the on-cycle EL enhancement of a single device remains stable after 10 000 pulses at 9 V, as shown in Fig. S7 within the Supplemental Material [29]. The current-density–voltage–luminance (*J-V-L*) curves of TSF OLEDs under dc and pulsed operation are further plotted by obtaining the injected current and on-cycle EL intensity

taken from the transient current and EL responses curves (Fig. S6 within the Supplemental Material [29]) [35]. Short-pulse operation and the small size characteristics of microsized OLEDs ensure repeatability of the *J-V-L* curve (Fig. S8 within the Supplemental Material [29]). Notably, the EL intensity under the pulsed operation surpasses that under the dc operation, and this enhancement increases as the current density rises [Fig. 1(e)]. On the other hand, the change in current density under the pulsed operation can be neglected compared to the evident change in the EL intensity. This phenomenon suggests that the enhancement of on-cycle EL does not result from reduced Joule heating under the pulsed operation (Fig. S9 within the Supplemental Material [29]) [36], but rather arises from the suppression of triplet accumulation and annihilation during short pulses. As shown in Fig. 1(f), the enhancement in EQE becomes more significantly at high on-cycle luminance, which is approximately 3% at 100 cd m^{-2}, 12% at approximately 1000 cd m^{-2}, and approximately 51% at 10 000 cd m^{-2}. Moreover, the on-cycle luminance is improved from 31 370 to 55 760 cd m^{-2} under a pulse operation of 10 V, indicating the effectiveness of the pulsed operation in suppressing efficiency roll-off in TSF OLEDs. Meanwhile, the enhancement of on-cycle EQE is positively correlated with current density, reaching a 100% improvement at 1 A cm^{-2} (Fig. S10 within the Supplemental Material [29]). Note

that the pulse operation at a low duty cycle increases the on-cycle EQE significantly, but decreases the EQE for integrated luminance as it requires an extremely high current density (Fig. S11 within the Supplemental Material [29]).

C. Transient EL spectrum and exciton dynamics of TSF OLEDs

To further investigate the transient EL behavior of TSF OLEDs under pulsed excitation, streak camera measurements are employed to examine the spectral evolution of the transient EL. The transient EL spectra are depicted in Fig. 2(a), exhibiting a narrow-band characteristic consistent with the steady-state EL spectra (Fig. S12 within the Supplemental Material [29]). The EL spectrum of TSF OLEDs at time intervals of 0.5, 1.0, 2.0, and 3.0 μs are given in Fig. 2(b). The EL intensity exhibits a decelerated decline during the initial 2 μs following the onset of the pulse, and subsequently remains constant. The diminishing intensity in EL spectral over time is consistent with the transient EL intensity discussed in Fig. 1(e), which also arises from the exciton population evolution. Besides, the transient EL spectrum consistently exhibits an emission from the emitter, indicating the fast energy transfer process can be neglected compared to the RISC and triplet annihilation in TSF OLED. The transient PL spectra of the TSF
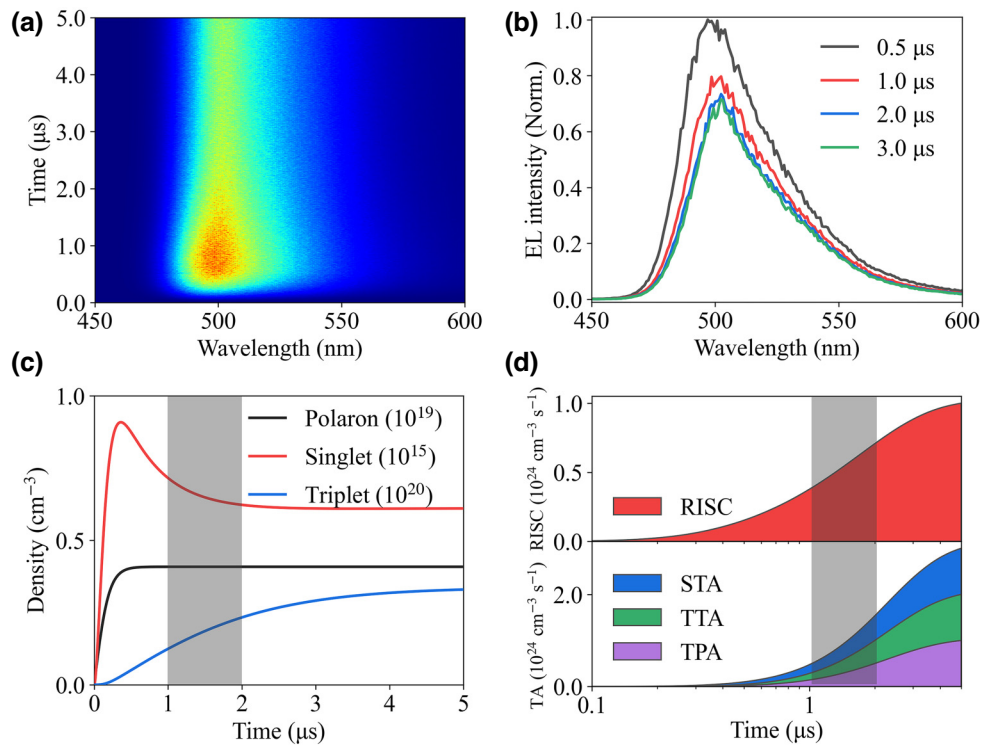

FIG. 2. (a) Transient EL spectra of TSF OLEDs operated under pulsed operation with a width of 5 μs, a repetition rate of 10 kHz, a duty ratio of 5%, and a current density of 1 A cm^{-2}. (b) The EL spectrum of TSF OLEDs under pulsed operation at various times. (c) Simulated temporal density of polarons, singlets, and triplets in TSF OLEDs at 1 A cm^{-2}. (d) The rate of RISC and triplet annihilation in TSF OLEDs.

film further confirms the rate of energy transfer is up to $10^8 \, \text{s}^{-1}$, which is much higher than that of RISC and triplet annihilation (Fig. S13 within the Supplemental Material [29]). Hence, in the exciton population evolution in TSF OLEDs [37–40], we can perform exciton dynamics simulations while simultaneously omitting the energy-transfer process to investigate and quantify triplet behavior in TSF OLEDs. The equations governing the temporal populations of polarons (n), singlets (S), and triplets (T) are given by written as

$$\frac{dn}{dt} = \frac{J(t)}{ed} - \gamma n^2, \text{ with } \gamma = \frac{e(\mu_e + \mu_h)}{\varepsilon_0 \varepsilon_r}, \quad (1)$$

where n is the polaron density, $J(t)$ is the current density as a function of time, e is the elementary charge, d is the width of the recombination zone, and γ is the Langevin recombination rate, ε_0 and ε_r is e the relative permittivity of EML and the permittivity of free space, respectively. μ_e and μ_h represent the mobility of electron and hole, respectively.

$$\frac{dS}{dt} = \frac{1}{4}\gamma n^2 - k_S S - k_{\text{ISC}}S + k_{\text{RISC}}T + \frac{1}{4}k_{\text{TTA}}T^2$$
$$- k_{\text{SSA}}S^2 - k_{\text{STA}}ST - 2k_{\text{SPA}}nS, \quad (2)$$

$$\frac{dT}{dt} = \frac{3}{4}\gamma n^2 - k_T T + k_{\text{ISC}}S - k_{\text{RISC}}T - \frac{5}{4}k_{\text{TTA}}T^2$$
$$- k_{\text{STA}}ST - 2k_{\text{TPA}}nT, \quad (3)$$

where S and T represent singlet and triplet density, k_S, k_{ISC}, k_{RISC}, k_{SSA}, k_{STA}, k_{SPA}, k_{TTA}, k_{TPA} are the rate constants of radiative decay of singlets, nonradiative decay of triplets, intersystem crossing (ISC), reverse intersystem crossing (RISC), singlet-singlet annihilation (SSA), singlet-triplet annihilation (STA), singlet-polaron annihilation (SPA), triplet-triplet annihilation (TTA), and triplet-polaron annihilation (TPA), respectively.

By modeling the results of transient EL response, the exciton population evolution of TSF OLEDs is shown in Fig. 2(c). The singlet exciton reaches its maximum density at about 250 ns and then gradually decreases to the steady state within 2 μs, which is suppressed by the triplet annihilation. Meanwhile, the accumulation of triplets over 5 μs results in a significant change in the competition between RISC and triplet annihilation, which is due to the linear and quadratic dependence on triplets of monomolecular and bimolecular processes. The rates of different decay routes of triplets are shown in Fig. 2(d). The results indicates that within the initial 1 μs, the triplet exciton density is low so that the RISC process dominates over triplet annihilation. As the triplets accumulate, the triplet annihilation begins to dominate over the RISC process within 1–2 μs, consistent with the relaxation from maximum EL intensity to steady state. The relative contributions to the depopulation of the singlets are also investigated (Fig. S14 within

the Supplemental Material [29]), confirming that the triplet annihilation is the main quenching factor compared to other decay routes, such as SSA and SPA.

D. Magnetic field effect of TSF OLEDs and the competition between RISC and triplet annihilation

The competition between RISC and triplet accumulation affects the spin-conversion process and the exciton interaction, allowing for the observation of changes in EL intensity upon the applied magnetic field (MEL) [41–46], as shown in Fig. 3(a). When the current density is low ($10^{-3} \, \text{A cm}^{-2}$), the transition from the triplet exciton to the singlet exciton via RISC dominates. When an external magnetic field is applied, the degeneracy of the triplet state is lift and the spin-conversion process is restricted, resulting in less bright singlets and a negative MEL [47]. With the current density increases from 10^{-3} to $10^{-1} \, \text{A cm}^{-2}$, the signal of MEL shows a transition from negative to positive indicating that the RISC is gradually quenched. As the current density further increases to $1 \, \text{A cm}^{-2}$, the triplet annihilation dominates. When an external magnetic field is applied, the triplet-triplet annihilation will be suppressed [48], leading to an improved utilization of triplets and a positive MEL. Interestingly, the dependence of EL intensity and MEL (measured at 300 mT) on current density also shows three components as shown in Fig. 3(b): (1) when the current density is lower than $5 \times 10^{-3} \, \text{A cm}^{-2}$, the EL intensity rapidly increases with the current density, which is caused by the dominance of RISC process and manifested as a negative MEL; (2) when the current density is in the range of $5 \times 10^{-3} \, \text{A cm}^{-2}$ to $2 \times 10^{-2} \, \text{A cm}^{-2}$, the rate of increment in EL intensity slows down, which is attributed to the balanced competition between RISC and triplet annihilation and manifested as a positive MEL; (3) when the current density is higher than $2 \times 10^{-2} \, \text{A cm}^{-2}$, the EL intensity slowly increases, which is due to the dominance of triplet annihilation and manifested as a positive MEL with an increasing high-field component.

Served as an indication of the competition between RISC and triplet annihilation, time-resolved MEL (TRMEL) of TSF OLEDs at a current density of $1 \, \text{A} \, \text{cm}^{-2}$ is measured as shown in Fig. 3(c). The amplitude of MEL increases over time, which is attributed to the enhancement of triplet annihilation over time. Notably, the negative MEL observed within 0.5 μs following the onset of the pulse indicates that the RISC route can still dominate over triplet annihilation during the initial hundreds of nanoseconds even under high current injection (Fig. S15 within the Supplemental Material [29]). In addition, TRMEL of the EL decay is also measured as shown in Fig. 3(d), which consists of a prompt component (<5 μs) with positive signal attributed to triplet annihilation, and a delayed component with negative signal due to RISC. The TRMEL corresponds to the decay of triplets after
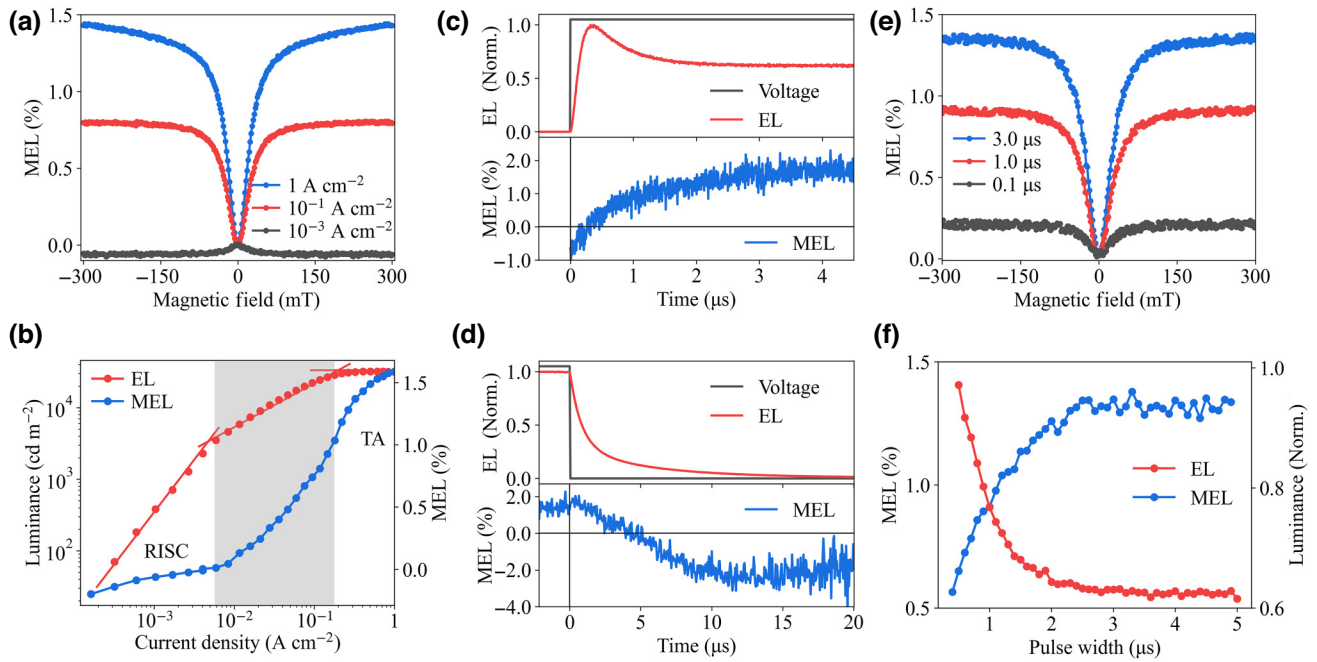
FIG. 3.   (a) MEL curves measured from the TSF OLEDs at various current densities. (b) The EL intensity and MEL curves of TSF OLEDs at various current densities. The MEL curve is measured at 300 mT. Pulse excitation in (a),(b): pulse width of 0.5 μs, repetition frequency of 100 kHz, duty ratio of 5%. (c) Time-resolved MEL of the EL response of TSF OLEDs at a current density of 1 A cm^{-2}. (d) Time-resolved MEL of the EL decay of TSF OLEDs at a current density of 1 A cm^{-2}. Pulse excitation in (c),(d): pulse width of 5 μs, repetition frequency of 10 kHz, duty ratio of 5%. (e) The MEL dependence on pulse widths of TSF OLEDs under electrical pumping at a current density of 1 A cm^{-2}. (f) Pulse-width-dependent MEL and EL intensity of TSF OLEDs at a current density of 1 A cm^{-2}.

the pulse ends, where the high-density triplets (<5 μs) lead to the dominance of triplet annihilation, which is also reflected by the dependence of EL intensity on pulse intervals (Fig. S16 within the Supplemental Material [29]). As shown in Fig. 3(e), the rapid decrease of MEL with decreasing pulse width confirms the effective manipulation of triplet excitons by pulsed operations, leading to a suppressed triplet annihilation. Meanwhile, the effectiveness of pulsed operation in triplet management is evident in the increased EL intensity with decreasing pulse width as shown in Fig. 3(f). The MEL and EL amplitude maintain when the pulse width exceeds 2 μs, which corresponds to the time interval dominated by triplet accumulation and annihilation as depicted in Fig. 2(d).

E. Universality of the pulsed operation and simulation results

As discussed above, using the pulsed operation to suppress the efficiency roll-off is based on reducing the triplet accumulation and leading to the dominance of RISC over triplet annihilation. In order to validate the universality of the pulsed operation and further investigate the impact of the RISC rate on the pulsed operation, 2CzPN with slower RISC rate (Fig. S17 within the Supplemental Material [29]) is chosen as a comparison. The difference between dc and pulsed operations of 2CzPN-sensitizing OLEDs is

also studied by the transient current and EL response, as shown in Fig. 4(a). Compared to the relatively gradual EL peak of 5CzBN-sensitizing OLEDs, the EL peak of 2CzPN-sensitizing OLEDs exhibits a steeper decline and a higher peak-to-steady-state ratio, as shown in Fig. 4(b). We have utilized numerical simulations based on exciton dynamics to determine the pulse width required for TSF OLEDs under different current densities and RISC rates as shown in Fig. 4(c), indicating that the required pulse width decreases with increasing RISC rate and current density, corresponding to the experimental observation of the prevalence of triplet annihilation in the competition with RISC as the current density increases. As shown in Fig. 4(d), the pulsed operation also enhances the on-cycle luminance of the 2CzPN-sensitizing OLEDs from 16 050 to 46 560 cd m^{-2} at an amplitude of 10 V, along with a significant improvement in the efficiency roll-off (Fig. S18 within the Supplemental Material [29]). The on-cycle EL improvement of two TSF OLEDs under various current densities is extracted and illustrated in Fig. 4(e), showing a more significant EL enhancement in 2CzPN-sensitizing OLEDs. This is due to the fact that slower RISC rates in 2CzPN lead to more severe triplet state accumulation; therefore, the performance improvement of TSF OLEDs is more pronounced with pulse operation. The performance improvement is also simulated based on exciton dynamics as shown in Fig. 4(f) and Fig. S19 within
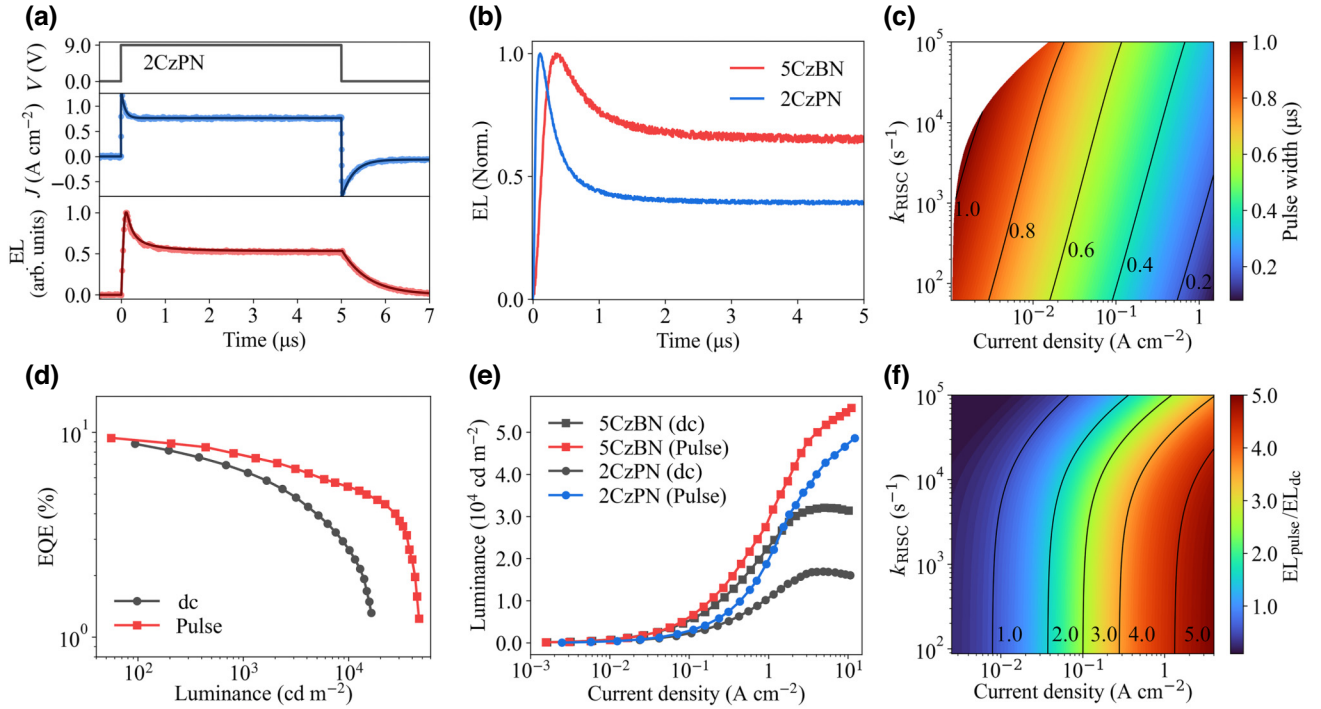
FIG. 4. (a) The current and EL responses of 2CzPN-sensitzing OLEDs under a pulse with an intensity of 9 V. Pulse excitation: pulse width of 5 μs, repetition frequency of 10 kHz, duty ratio of 5%. (b) Transient EL responses of 5CzBN- and 2CzPN-sensitizing OLEDs. (c) Pulse width versus current density, as a function of RISC rate simulated by exciton dynamics. (d) Plots of EQE versus on-cycle luminance in 2CzPN-sensitizing OLEDs under dc and pulsed operation. Pulse excitation: pulse width of 0.5 μs, repetition frequency of 100 kHz, duty ratio of 5%. (e) Plots of on-cycle luminance versus current density in 5CzBN- and 2CzPN-sensitizing OLEDs under dc and pulsed operation. (f) The improvement of on-cycle EL intensity under pulsed operation simulated by exciton dynamics.

the Supplemental Material [29], indicating that the pulsed operation is more effective in TSF OLEDs with a lower RISC rate and at a higher current density.

III. CONCLUSION

In conclusion, we observed that the on-cycle EQE can be improved by 100% under pulsed operation at a high current density of 1 A cm^{-2}, accompanied by a significant increasement in the on-cycle luminance from 31 370 to 55 760 cd m^{-2} at an amplitude of 10 V. The transient EL responses of TSF OLEDs show a triplet annihilation-induced EL peak within 1–2 μs, which indicates the dominance of triplet annihilation over RISC due to the accumulation of long-lived triplets. Based on the results, exciton dynamics simulation is performed indicating the singlet exciton reaches the peak intensity within a few hundred nanoseconds, while the accumulation of long-lived triplet exciton lasts over 5 μs. The accumulation of triplets significantly enhances the bimolecular triplet annihilation, which is revealed by the dependence of MFE on the current densities. Using MFE as the indication of the competition between RISC and triplet annihilation, the TRMEL results confirm the gradual dominance of triplet annihilation within the initial 2 μs under electrical pumping.

The negative dependence of MEL on the pulse width further indicates the effectiveness of the pulsed operation on reducing triplet annihilation. Based on the exciton dynamics simulation, we obtain the required pulse width and the improvement of EL in TSF OLEDs under pulsed operation in terms of the current density and RISC rate. Our study provides reference for utilizing pulsed operations to suppress the efficiency roll-off in TSF OLEDs and may benefit for their applications in electrically pumped lasers, healthcare lighting, and so on.

APPENDIX: EXPERIMENTAL METHODS

1. Micro-TSF-OLED fabrication

In this work, the fabrication process of micro TSF OLEDs involves the following steps: (1) the 150-nm-thick

indium-tin-oxide (ITO) substrates undergo a cleaning process involving toluene, acetone, and tert-butanol, each for a duration of 20 min, utilizing an ultrasonic bath. Subsequently, they are dried at 110 °C prior to oxygen plasma treatment; (2) the polymethyl methacrylate (PMMA) solution is prepared by dissolving PMMA in chlorobenzene (10 mg/ml). Subsequently, the PMMA solution is spin-coated onto an ITO substrate at 3000 rpm to obtain a PMMA thin film with a thickness of 100 nm; (3) then, the ITO glass with a spin-cast layer of PMMA film is transferred to the SEM (NOVA NANO 450) equipped with a nanofabrication accessory for electron-beam lithography (processing parameters: the electron acceleration voltage is 30 kV, the electron beam current is 84 μA, and the electron-beam dose is 5,500 μC cm^{-2}); (4) after etching, the sample is immersed in the developer solution (methyl isobutyl ketone: isopropyl alcohol = 1:3) for 30 s to dissolve the etched areas. Then, the sample is immersed in the fixative solution (isopropyl alcohol) for 30 s to stabilize the pattern, resulting in a PMMA template for the fabrication of micro OLEDs; (5) a deposit layer of N,N′-Bis(naphthalen-1-yl)-N,N′-bis(phenyl)benzidine (NPD) is used as the hole transport layer (HTL), and a deposited layer of 90 wt% 4,4′-Bis(9-carbazolyl)-1,1′-biphenyl (CBP) as the host, 10 wt% 2,3,4,5,6-penta(carbazol-9-yl)benzonitrile (5CzBN) as the TADF sensitizer and 1 wt% 2,12-di-tert-butyl-5,9-bis(4-(tert-butyl) phenyl)-5,9-dihydro-5,9-diaza-13b-boranaphtho[3,2,1-de]anthracene (t-DABNA) is used as an emitting layer, a deposit layer of 1,3,5-Tris(1-phenyl-1H-benzimidazol-2-yl)-benzene (TPBi) is used as an electron transport layer (ETL); a thermally evaporated layer of LiF/Al cathode was capped on top.

2. The characterization of TSF OLEDs

The steady-state (dc) current-density–voltage–luminance (*J-V-L*) characteristics of the TSF OLEDs are measured using a Keithley 2450 source measure unit, a calibrated photomultiplier tube (Hamamatsu H10721, with a rise time of 0.57 ns), a wide bandwidth transimpedance

amplifier (Hamamatsu C11184) and a DMM 6500 multimeter. The pulsed operation is performed using a pulse generator (Quantum Composer, QC9522) amplified by a custom power amplifier (Aigtek ATA2000), which have a rated rise and fall time <10 ns. For the *J-V-L* characteristics and MEL measurements, a pulse with a width of 0.5 μs, a repetition rate of 100 kHz, and a duty ratio of 5% is applied; for the time-resolved measurements, a pulse with a width of 5 μs, a repetition rate of 10 kHz and a duty ratio of 5% is applied. The current is determined by measuring the voltage across a 50-Ω termination resistor amplified by a high-speed amplifier and detected using an oscilloscope (Tektronix MDO 4000, with 1-GHz frequency range and 2.5-Gs s^{-1} sampling rate). The transient EL signals of the samples are extracted using a H10721 photomultiplier tube, then transformed into electrical signal using a C11184 transimpedance amplifier and finally collected using the MDO 4000 oscilloscope. The EQE and EL intensity of TSF OLEDs under the pulsed operation is determined from the average value during the pulse width. And the spectrally resolved transient EL spectra are collected using a Hamamatsu C13410 streak camera (5-ps temporal resolution).

The transient current response of TSF OLEDs [Fig. 1(d)] was fitted using the transient response curve of the device's *RC* effect as follows [25]:

$$V_c(t) = V_{\text{in}}(t) - R_s I(t), \tag{A1}$$

$$C\frac{dV_c(t)}{dt} + V_c(t)\left(\frac{1}{R_{\text{layer}}} + \frac{1}{R_s}\right) - \frac{V_{\text{in}}(t)}{R_s} = 0. \tag{A2}$$

The parameters are as follows: $V_c = 9$ V, $R_s = 50$ Ω, $R_{\text{layer}} = 200$ Ω, $C = 100$ pF. The transient electroluminescence response of TSF OLEDs was fitted using the exciton dynamics equation, Eqs. (1)–(3). The parameters used for exciton dynamics simulations are shown in Table I.

3. The magnetic field effect measurements

For the MEL measurements, the device is transferred to a vacuum chamber of cryostat (Oxford OptistatDry BLV)

TABLE I.　Key parameters and rate constants obtained by fitting.

	2CzPN-sensitizing OLEDs		5CzBN-sensitizing OLEDs	
	Initial value	Fitted value	Initial value	Fitted value
k_S(s^{-1})	3.2×10^7 [49]	2.8×10^7	7.4×10^7 s^{-1} [50]	7.4×10^7 s^{-1}
k_T(s^{-1})	8.1×10^2 [49]	4.1×10^2	1.1×10^4 s^{-1} [50]	2.1×10^4 s^{-1}
k_{ISC}(s^{-1})	3.1×0^7 [49]	7.1×10^7	2.0×10^8 s^{-1} [50]	5.1×10^8 s^{-1}
k_{RISC}(s^{-1})	5.6×10^3 [49]	4.8×10^3	8.8×10^4 s^{-1} [51]	7.9×10^4 s^{-1}
k_{SSA}(cm^{3}s^{-1})	6.3×10^{-12}	3.7×10^{-12}	1.2×10^{-11} s^{-1}	2.5×10^{-11}
k_{STA}(cm^{3}s^{-1})	2×10^{-10} [49]	1.5×10^{-9}	5.6×10^{-10} s^{-1}	1.4×10^{-9}
k_{SPA}(cm^{3}s^{-1})	4.2×10^{-10}	1.1×10^{-9}	2.1×10^{-10} s^{-1}	2.1×10^{-10}
k_{TTA}(cm^{3}s^{-1})	5×10^{-15} [49]	5×10^{-14}	2.5×10^{-15} s^{-1}	6.1×10^{-14}
k_{TPA} (cm^{3}s^{-1})	7.6×10^{-12}	3.5×10^{-13}	5.2×10^{-13} s^{-1}	4.2×10^{-13}

that is placed in a magnetic field B provided by an electromagnet (Eastchanging EM4) with magnetic field up to 300 mT. For dc measurements, the device is excited by the Keithley 2450 source measurement unit; while for pulse measurements, it is excited by the pulse generator. The EL signals extracted using a H10721 photomultiplier tube, then transformed into electrical signal using a C11184 transimpedance amplifier and finally collected using the MDO 4000 oscilloscope. The MEL is defined as MEL(B) = [EL(B)/EL(0) × 100%] measured under the dc and pulsed operation. The external magnetic field was swept at a rate of 10 mT s^{-1} in one direction and back for several cycles to improve the SNR of MEL(B).

4. The parameters used for exciton dynamics simulations

The simulated exciton population dynamics using the experimental parameters mentioned above are presented in Table I. The transient processes under optical and electrical pulsing are commonly considered to be alike. The rates of the monomolecular processes, such as k_s, k_T, k_{ISC}, and k_{RISC}, are extracted from the photophysical characteristics of TSF films and the corresponding literature. While the k_{SSA}, k_{STA}, k_{SPA}, k_{TTA}, and k_{TPA} are bimolecular recombination rates. Since the exciton annihilation process commonly occurs between the host and the dopant [40], we use the parameters reported in the literature for the TADF sensitizer in our simulations.

---

[1] G. Hong, X. Gan, C. Leonhardt, Z. Zhang, J. Seibert, J. M. Busch, and S. Bräse, A brief history of OLEDs—emitter development and industry milestones, Adv. Mater. **33,** 2005630 (2021).

[2] N. C. Giebink and S. R. Forrest, Quantum efficiency roll-off at high brightness in fluorescent and phosphorescent organic light emitting diodes, Phys. Rev. B **77,** 235215 (2008).

[3] D. Li and L.-S. Liao, Highly efficient deep-red organic light-emitting diodes using exciplex-forming co-hosts and thermally activated delayed fluorescence sensitizers with extended lifetime, J. Mater. Chem. C **7,** 9531 (2019).

[4] M. Jakoby, B. S. Richards, U. Lemmer, and I. A. Howard, Investigations of singlet and triplet diffusion in thermally activated delayed-fluorescence emitters: Implications for hyperfluorescence, Phys. Rev. B **100,** 045303 (2019).

[5] C. Yin, D. Zhang, Y. Zhang, Y. Lu, R. Wang, G. Li, and L. Duan, High-efficiency narrow-band electro-fluorescent devices with thermally activated delayed fluorescence sensitizers combined through-bond and through-space charge transfers, CCS Chem. **2,** 1268 (2020).

[6] C.-Y. Chan, M. Tanaka, Y.-T. Lee, Y.-W. Wong, H. Nakanotani, T. Hatakeyama, and C. Adachi, Stable pure-blue hyperfluorescence organic light-emitting diodes with high-efficiency and narrow emission, Nat. Photonics **15,** 203 (2021).

[7] E. Kim, J. Park, M. Jun, H. Shin, J. Baek, T. Kim, S. Kim, J. Lee, H. Ahn, J. Sun, S.-B. Ko, S.-H. Hwang, J. Lee, C. Chu, and S. Kim, Highly efficient and stable deep-blue organic light-emitting diode using phosphor-sensitized thermally activated delayed fluorescence, Sci. Adv. **8,** eabq1641 (2022).

[8] C. Yin, Y. Zhang, T. Huang, Z. Liu, L. Duan, and D. Zhang, Highly efficient and nearly roll-off–free electrofluorescent devices via multiple sensitizations, Sci. Adv. **8,** eabp9203 (2022).

[9] Y. Tian, Y.-Z. Shi, X.-C. Fan, S.-G. Wan, X.-M. Wang, K. Wang, J. Yu, X.-H. Zhang, and C.-Q. Ye, Exploring the key factors of TADF materials as sensitizers: Toward high-performance triplet fusion upconversion, Adv. Opt. Mater. **11,** 2300504 (2023).

[10] K. Sato, K. Shizu, K. Yoshimura, A. Kawada, H. Miyazaki, and C. Adachi, Organic luminescent molecule with energetically equivalent singlet and triplet excited states for organic light-emitting diodes, Phys. Rev. Lett. **110,** 247401 (2013).

[11] K. Shizu, M. Uejima, H. Nomura, T. Sato, K. Tanaka, H. Kaji, and C. Adachi, Enhanced electroluminescence from a thermally activated delayed-fluorescence emitter by suppressing nonradiative decay, Phys. Rev. Appl. **3,** 014001 (2015).

[12] S. Wehrmeister, L. Jäger, T. Wehlus, A. F. Rausch, T. C. G. Reusch, T. D. Schmidt, and W. Brütting, Combined electrical and optical analysis of the efficiency roll-off in phosphorescent organic light-emitting diodes, Phys. Rev. Appl. **3,** 024008 (2015).

[13] R. Saxena, T. Meier, S. Athanasopoulos, H. Bässler, and A. Köhler, Kinetic Monte Carlo study of triplet-triplet annihilation in conjugated luminescent materials, Phys. Rev. Appl. **14,** 034050 (2020).

[14] M. Hasan, A. Shukla, M. Mamada, C. Adachi, S.-C. Lo, and E. B. Namdas, Correlating exciton dynamics of thermally activated delayed-fluorescence emitters to efficiency roll-off in OLEDs, Phys. Rev. Appl. **18,** 054082 (2022).

[15] B. van der Zee, Y. Li, G.-J. A. H. Wetzelaer, and P. W. M. Blom, Triplet-polaron-annihilation-induced degradation of organic light-emitting diodes based on thermally activated delayed fluorescence, Phys. Rev. Appl. **18,** 064002 (2022).

[16] M. Hasan, A. Shukla, V. Ahmad, J. Sobus, F. Bencheikh, S. K. M. McGregor, M. Mamada, C. Adachi, S.-C. Lo, and E. B. Namdas, Exciton–exciton annihilation in thermally activated delayed fluorescence emitter, Adv. Funct. Mater. **30,** 2000580 (2020).

[17] Y. Zaushitsyn, K. G. Jespersen, L. Valkunas, V. Sundström, and A. Yartsev, Ultrafast dynamics of singlet-singlet and singlet-triplet exciton annihilation in poly(3-2′-methoxy-5′octylphenyl)thiophene films, Phys. Rev. B **75,** 195201 (2007).

[18] L.-S. Cui, A. J. Gillett, S.-F. Zhang, H. Ye, Y. Liu, X.-K. Chen, Z.-S. Lin, E. W. Evans, W. K. Evans, W. K. Myers, T. K. Ronson, H. Nakanotani, S. Reineke, J.-L. Bredas, C. Adachi, and R. H. Friend, Fast spin-flip enables efficient and stable organic electroluminescence from charge-transfer states, Nat. Photonics **14,** 636 (2020).

[19] Y. X. Hu, J. Miao, T. Hua, Z. Huang, Y. Qi, Y. Zou, Y. Qiu, H. Xia, H. Liu, X. Cao, and C. Yang, Efficient

selenium-integrated TADF OLEDs with reduced roll-off, Nat. Photonics **16**, 803 (2022).

[20] S. O. Jeon, K. H. Lee, J. S. Kim, S.-G. Ihn, Y. S. Chung, J. W. Kim, H. Lee, S. Kim, H. Choi, and J. Y. Lee, High-efficiency, long-lifetime deep-blue organic light-emitting diodes, Nat. Photonics **15**, 208 (2021).

[21] D. Liu, Y. He, W. Qiu, X. Peng, M. Li, D. Li, J. Pu, J. Yang, Y. Gan, G. Yang, G. Sun, C. Shen, X. Cai, and S.-J. Su, Management of host–guest triplet exciton distribution for stable, high-efficiency, low roll-off solution-processed blue organic light-emitting diodes by employing triplet-energy-mediated hosts, Adv. Funct. Mater. **33**, 2301327 (2023).

[22] S. Xiao, X. Qiao, C. Lin, Y. Li, S. Qin, R. Guo, L. Wang, Y. Ma, and D. Ma, Revealing the evolution processes of excitons on high energy level in anthracene-based OLEDs, Adv. Funct. Mater. **32**, 2207123 (2022).

[23] M. A. Baldo, C. Adachi, and S. R. Forrest, Transient analysis of organic electrophosphorescence. II. Transient analysis of triplet-triplet annihilation, Phys. Rev. B **62**, 10967 (2000).

[24] K. Yoshida, J. Gong, A. L. Kanibolotsky, P. J. Skabara, G. A. Turnbull, and I. D. W. Samuel, Electrically driven organic laser using integrated OLED pumping, Nature **621**, 746 (2023).

[25] V. Ahmad, J. Sobus, M. Greenberg, A. Shukla, B. Philippa, A. Pivrikas, G. Vamvounis, R. White, S.-C. Lo, and E. B. Namdas, Charge and exciton dynamics of OLEDs under high voltage nanosecond pulse: towards injection lasing, Nat. Commun. **11**, 4310 (2020).

[26] D. G. Bossanyi, Y. Sasaki, S. Wang, D. Chekulaev, N. Kimizuka, N. Yanai, and J. Clark, Spin statistics for triplet-triplet annihilation upconversion: Exchange coupling, intermolecular orientation, and reverse intersystem crossing, JACS Au **1**, 2188 (2021).

[27] C. Li, L. Duan, D. Zhang, and Y. Qiu, Thermally activated delayed fluorescence sensitized phosphorescence: A strategy to break the trade-off between efficiency and efficiency roll-off, ACS Appl. Mater. Interfaces **7**, 15154 (2015).

[28] Y. Zhang and S. R. Forrest, Triplets contribute to both an increase and loss in fluorescent yield in organic light emitting diodes, Phys. Rev. Lett. **108**, 267404 (2012).

[29] See Supplemental Material at http://link.aps.org/supplemental/10.1103/PhysRevApplied.21.014039 for detailed description of methods and materials and Figs. S1–S19.

[30] L. Zeng, A. C. Chime, M. Chakaroun, S. Bensmida, H. Nkwawo, A. Boudrioua, and A. P. A. Fischer, Electrical and optical impulse response of high-speed micro-OLEDs under ultrashort pulse excitation, IEEE Trans. Electron Devices **64**, 2942 (2017).

[31] F. Xu Fa, J. Li Yong, Y. Lv, H. Dong, X. Lin, K. Wang, J. Yao, and S. Zhao Yong, Flat-panel laser displays based on liquid crystal microlaser arrays, CCS Chem. **2**, 369 (2020).

[32] C. Qiao, C. Zhang, Z. Zhou, J. Yao, and S. Zhao Yong, An optically reconfigurable Förster resonance energy transfer process for broadband switchable organic single-mode microlasers, CCS Chem. **4**, 250 (2021).

[33] H. Dong, C. Zhang, W. Zhou, J. Yao, and Y. S. Zhao, Differential polymer chain scission enables free-standing microcavity laser arrays, Adv. Mater. **34**, 2107611 (2022).

[34] Y. Zhang, M. Whited, M. E. Thompson, and S. R. Forrest, Singlet–triplet quenching in high intensity fluorescent organic light emitting diodes, Chem. Phys. Lett. **495**, 161 (2010).

[35] H. Bao, C. Chen, Y. Cao, S. Chang, S. Wang, and H. Zhong. J. Phys. Chem. Lett. **14**, 1777 (2023).

[36] H. Kim, L. Zhao, J. S. Price, A. J. Grede, K. Roh, A. N. Brigeman, M. Lopez, B. P. Rand, and N. C. Giebink, Hybrid perovskite light emitting diodes under intense electrical excitation, Nat. Commun. **9**, 4893 (2018).

[37] Y. Li, S. Ying, X. Zhang, S. Xiao, D. Zhang, X. Qiao, D. Yang, J. Peng, D. Ma, and Low Threshold, High Q-factor optically pumped organic lasers and exciton dynamics in OLEDs under high current density: singlet–triplet annihilation effect and toward electrical injection lasing, J. Phys. Chem. C **126**, 16025 (2022).

[38] C. Zhao, W. Tian, Q. Sun, Z. Yin, J. Leng, S. Wang, J. Liu, K. Wu, and S. Jin, Trap-enabled long-distance carrier transport in perovskite quantum wells, J. Am. Chem. Soc. **142**, 15091 (2020).

[39] Q. Sun, C. Zhao, Z. Yin, S. Wang, J. Leng, W. Tian, and S. Jin, Ultrafast and high-yield polaronic exciton dissociation in two-dimensional perovskites, J. Am. Chem. Soc. **143**, 19128 (2021).

[40] D. Kasemann, R. Brückner, H. Fröb, and K. Leo, Organic light-emitting diodes under high currents explored by transient electroluminescence on the nanosecond scale, Phys. Rev. B **84**, 115208 (2011).

[41] L. He, M. Li, A. Urbas, and B. Hu, Magnetophotoluminescence line-shape narrowing through interactions between excited states in organic semiconducting materials, Phys. Rev. B **89**, 155304 (2014).

[42] Y. Xu, X. Liang, X. Zhou, P. Yuan, J. Zhou, C. Wang, B. Li, D. Hu, X. Qiao, X. Jiang, L. Liu, S.-J. Su, and D. Ma, Highly efficient blue fluorescent OLEDs based on upper level triplet-singlet intersystem crossing, Adv. Mater. **31**, e1807388 (2019).

[43] X. Liu, H. Popli, O. Kwon, H. Malissa, X. Pan, B. Park, B. Choi, S. Kim, E. Ehrenfreund, C. Boehme, and Z. V. Vardeny, Isotope effect in the magneto-optoelectronic response of organic light-emitting diodes based on donor-acceptor exciplexes, Adv. Mater. **32**, e2004421 (2020).

[44] C. Zhao, F. Zhao, K. Wang, H. Yu, T. Huang, R. Wang, C. Zhang, B. Hu, and L. Duan, Stabilization of blue emitters with thermally activated delayed fluorescence by the steric effect: A case study by means of magnetic field effects, Phys. Rev. Appl. **14**, 034059 (2020).

[45] J. Xu, X. Tang, X. Zhao, H. Zhu, F. Qu, and Z. Xiong, Abnormal reverse intersystem crossing of polaron-pair states and its conversion to intersystem crossing via the regulation of intermolecular electron-hole spacing distance, Phys. Rev. Appl. **14**, 024011 (2020).

[46] X. Guo, P. Yuan, J. Fan, X. Qiao, D. Yang, Y. Dai, Q. Sun, A. Qin, B. Z. Tang, and D. Ma, Unraveling the important role of high-lying triplet-lowest excited singlet transitions in achieving highly efficient deep-blue AIE-based OLEDs, Adv. Mater. **33**, 2006953 (2021).

[47] P. Chen, Z. Xiong, Q. Peng, J. Bai, S. Zhang, and F. Li, Magneto-electroluminescence as a tool to discern the origin

of delayed fluorescence: Reverse intersystem crossing or triplet-triplet annihilation?, Adv. Opt. Mater. **2,** 142 (2014).

[48] Z. Zhou, R. Chen, P. Jin, J. Hao, W. Wu, B. Yin, C. Zhang, and J. Yao, Interplay between singlet and triplet excited states in interface exciplex OLEDs with fluorescence, phosphorescence, and TADF emitters, Adv. Funct. Mater. **33,** 2211059 (2023).

[49] K. Masui, H. Nakanotani, and C. Adachi, Analysis of exciton annihilation in high-efficiency sky-blue organic light-emitting diodes with thermally activated delayed fluorescence, Org. Electron. **14,** 2721 (2013).

[50] S. Tanimoto, T. Suzuki, H. Nakanotani, and C. Adachi, Thermally activated delayed fluorescence from pentacarbazorylbenzonitrile, Chem. Lett. **45,** 770 (2016).

[51] Hiroki Noda, Hajime Nakanotani, and Chihaya Adachi, Excited state engineering for efficient reverse intersystem crossing, Sci. Adv. **4,** eaao6910 (2018).